Electronic Supplementary Information

Tailoring the framework composition of carbon nitride to improve the catalytic efficiency of stabilised palladium atoms

E. Vorobyeva,[a] Z. Chen,[a] S. Mitchell,[a] R. K. Leary,[b] P. Midgley,[b] J. M. Thomas,[b] R. Hauert,[c] E. Fako,[d] N. López[d] and J. Pérez-Ramírez*[a]

[a]*Institute for Chemical and Bioengineering, Department of Chemistry and Applied Biosciences, ETH Zurich, Vladimir-Prelog-Weg 1, CH-8093 Zurich, Switzerland. E-mail: jpr@chem.ethz.ch*

[b]*Department of Materials Science and Metallurgy, University of Cambridge, CB3 0FS Cambridge, United Kingdom.*

[c]*EMPA, Swiss Federal Laboratories for Materials Science and Technology, Uberlandstrasse 129, CH-8600 Dubendorf, Switzerland.*

[d]*Institute of Chemical Research of Catalonia (ICIQ) and The Barcelona Institute of Science and Technology, Av. Països Catalans 16, 43007 Tarragona, Spain.*

Table S1. Chemical composition of the carriers studied.

Carrier[a]	C (mol%)[b]	N (mol%)[b]	H (mol%)[b]	O (mol%)[b]	Chemical formula[c]
MCN	31.3 (29.6[c])	47.2 (48.9)	17.1 (17.7)	4.3 (3.7)	$C_3N_{4.9}H_{1.8}O_{0.373}$
MCN-BA-0.02	29.1 (28.8)	41.4 (43.9)	25.0 (26.5)	4.5 (0.8)	$C_3N_{4.6}H_{2.8}O_{0.083}$
MCN-BA-0.2	32.2 (32.1)	38.9 (41.8)	23.2 (24.9)	5.6 (1.0)	$C_3N_{3.9}H_{2.3}O_{0.097}$
MCN-BA-0.9	40.1 (40.7)	39.2 (42.5)	13.5 (14.7)	7.2 (1.9)	$C_3N_{3.1}H_{1.1}O_{0.139}$
MCN-TAP-0.2	30.6 (30.5)	40.9 (42.6)	23.5 (24.5)	5.0 (2.4)	$C_3N_{4.2}H_{2.4}O_{0.233}$
MCN-TAP-0.9	33.7 (33.7)	36.9 (38.9)	24.0 (25.2)	5.4 (2.2)	$C_3N_{3.5}H_{2.2}O_{0.191}$
BCN	33.9 (33.9)	51.4 (52.4)	12.9 (13.2)	1.8 (0.5)	$C_3N_{4.6}H_{1.2}O_{0.048}$
BCN-BA-0.9	38.5 (37.1)	39.0 (39.3)	22.4 (22.6)	4.3 (1.1)	$C_3N_{3.2}H_{1.8}O_{0.089}$
BTAP	44.4 (43.9)	38.8 (38.7)	16.6 (16.5)	1.6 (0.9)	$C_3N_{2.6}H_{1.1}O_{0.061}$
BBA	53.9 (51.1)	24.9 (24.2)	21.0 (20.5)	6.7 (4.2)	$C_3N_{1.4}H_{1.2}O_{0.247}$

[a] Carbon-doped carriers are coded *x-y-z*, where *x* designates the carrier morphology - bulk (BCN) or mesoporous (MCN), *y* denotes the dopant - barbituric acid (BA) or 2,4,6-triaminopyrimidine (TAP) and *z* indicates the cyanamide/dopant mass ratio - 0.02, 0.2 or 0.9. Two reference carriers were prepared by thermal treatment of BA (BBA) or TAP (BTAP), respectively. [b] Elemental analysis. [c] Corrected for the presence of adsorbed CO_2.

Table S2. Porous properties and crystal size of the carriers studied.

Carrier	V_{pore} ($cm^3\ g^{-1}$)[a]	S_{BET} ($m^2\ g^{-1}$)[b]	$d_{crystal}$ (nm)[c]
MCN	0.62	219	9
MCN-BA-0.02	0.80	260	6
MCN-BA-0.2	0.71	285	4
MCN-BA-0.9	0.82	383	2
MCN-TAP-0.2	0.84	327	8
MCN-TAP-0.9	1.31	402	2
BCN	0.03	9	11
BCN-BA-0.9	0.05	48	5
BTAP	0.00	6	6
BBA	0.05	45	2

[a] Volume of N_2 adsorbed at $p/p_0 = 0.96$. [b] BET method. [c] Scherrer equation applied to the (002) reflection.

Table S3. Metal content, speciation and oxidation state, and porosity of the Pd-containing catalysts.

Catalyst	Metal content (wt.%)[a]	Metal speciation[b]	Pd^{2+}/Pd^{4+} (-)[c]	V_{pore} ($cm^3\ g^{-1}$)[d]	S_{BET} ($m^2\ g^{-1}$)[e]
Pd-MCN	0.50 (0.95)	SA	0.53	0.62	232
Pd-MCN-BA-0.2	0.42 (1.35)	SA	0.45	0.71	278
Pd-MCN-BA-0.9	0.40 (1.84)	SA	0.24	0.75	348
Pd-MCN-TAP-0.2	0.53 (1.27)	SA	0.7	0.75	309
Pd-MCN-TAP-0.9	0.34 (1.76)	SA	1.04	0.96	273
Pd-BCN	0.44 (5.47)	SA, C	0.57	0.05	21
Pd-BCN-BA-0.9	0.50[f] (11.78)	SA, C	0.75	0.02	10
Pd-BTAP	0.50[f] (12.37)	SA, C	0.31	0.01	4
Pd-BBA	0.50[f] (10.03)	SA, C, NP	0.35	0.08	61

[a] ICP (in parenthesis, surface metal content determined by XPS). [b] SA: single atom, C: clusters ranging from a few to tens of atoms, NP: nanoparticles a few nanometers in diameter. [c] XPS analysis. [d] Volume of N_2 adsorbed at $p/p_0 = 0.96$. [e] BET method. [f] Nominal value.

Table S4. Adsorption energies of Pd for the stoichiometric and modified carriers.

	Adsorption energy (eV)[a]					
Position[b]	r-CN	r-CN-CH	r-CN-CO	n-CN	n-CN-CH	n-CN-CO
s	-2.04	-1.54	-1.12	-1.61	-1.30	-1.43
u	-2.14	-1.82	-1.12	-2.17	-1.89	-1.93
w	-2.10	-2.11	-2.16	-2.16	-2.16	-2.66

[a] Values with respect to gas-phase atoms. Samples coded according to the composition (CN - stoichiometric; CH - C-doped; CO - oxygen defective) and stacking arrangement (r - rotated; n - normal) illustrated in **Figure 13**. [b] Positions s, u and w, as defined in **Figure S14**.

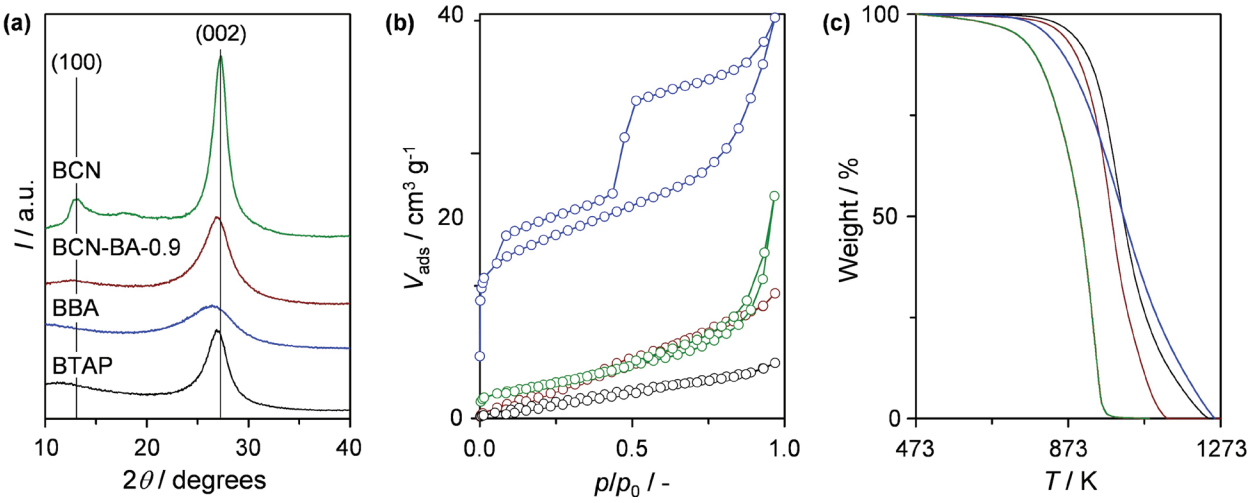

Figure S1. (a) Powder X-ray diffraction patterns, (b) N_2 isotherms and (c) thermogravimetric analysis profiles in air of the bulk carriers.

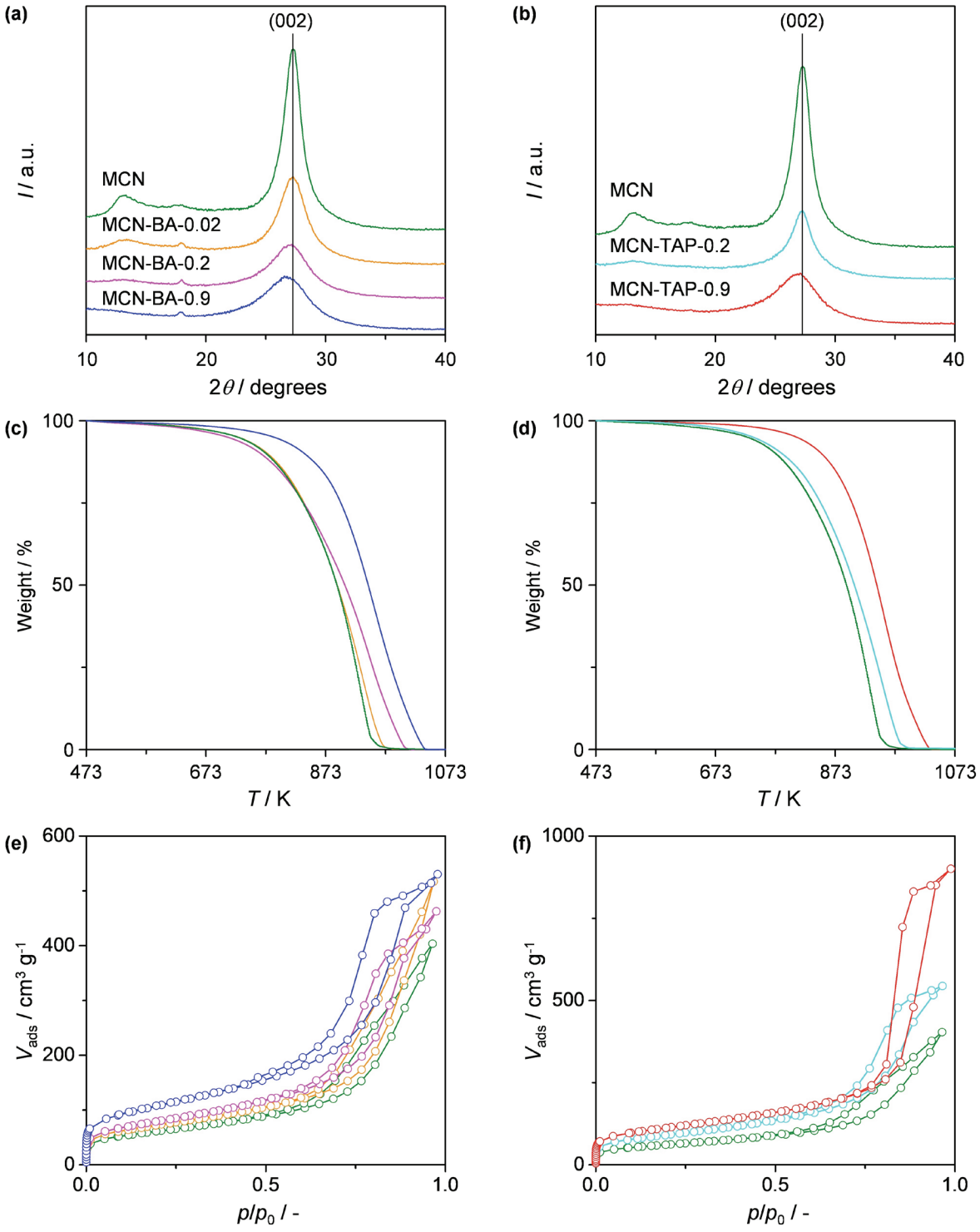

Figure S2. (a,b) Powder X-ray diffraction patterns, (c,d) thermogravimetric analysis profiles in air and (e,f) N_2 isotherms of MCN and the mesoporous C-doped carriers modified with BA and TAP.

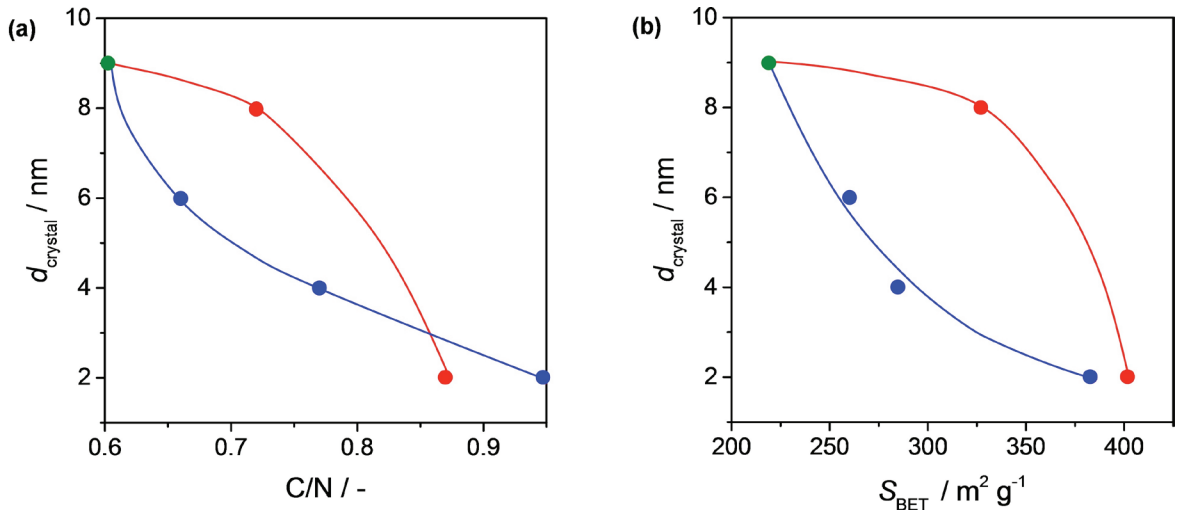

Figure S3. Correlations of the crystal size with (a) the C/N ratio and (b) the BET surface area of MCN (green symbol) and the mesoporous C-doped carriers modified with BA (blue symbols) and TAP (red symbols), respectively.

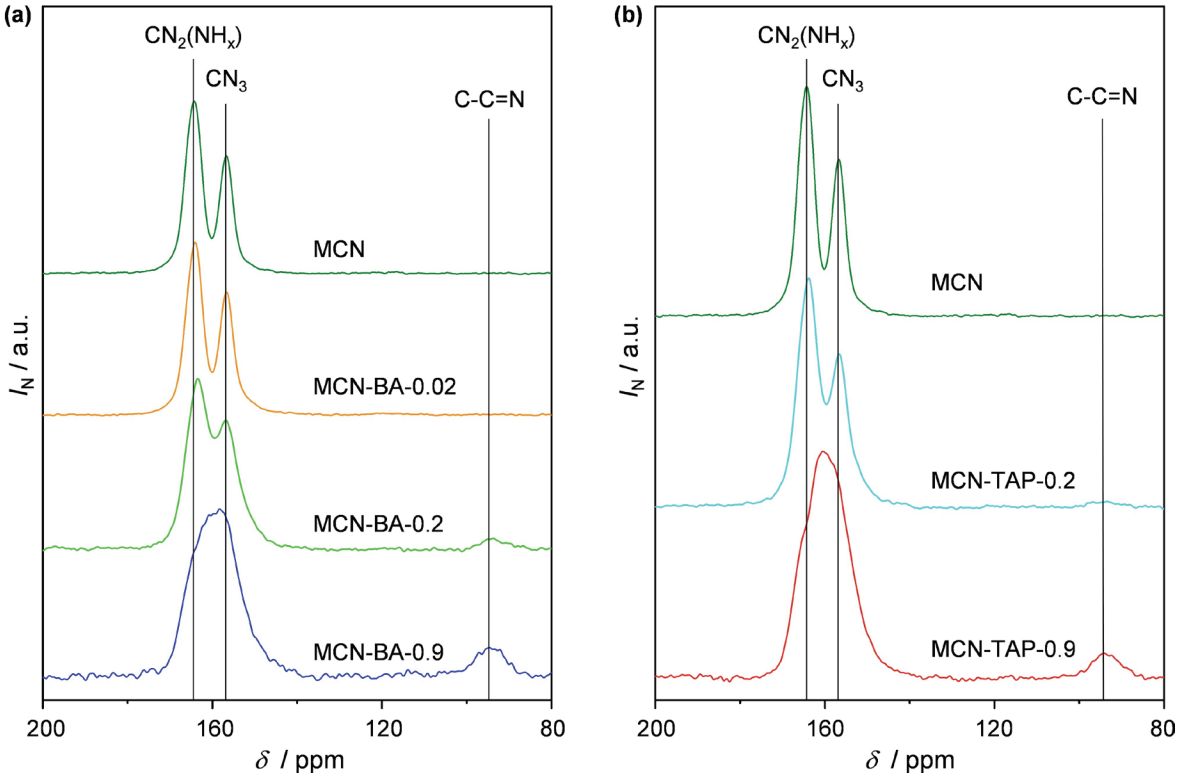

Figure S4. Comparison of ^{13}C solid-state cross-polarisation/magic angle spinning nuclear magnetic resonance spectra of MCN and the mesoporous C-doped carriers modified with BA and TAP.

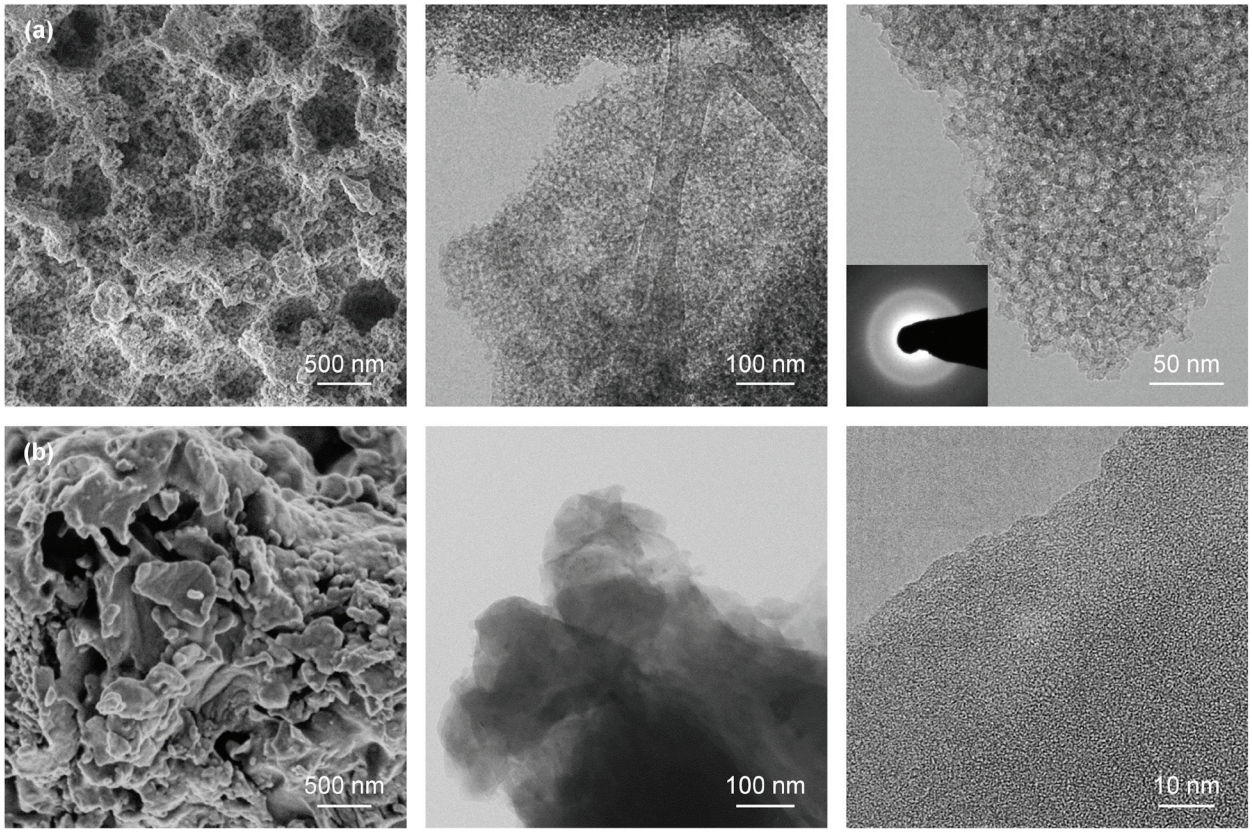

Figure S5. Scanning (left) and transmission electron (centre and right) micrographs of the metal-free MCN (top row) and BCN (bottom row) carriers. The selected area diffraction pattern of MCN (shown inset) reveals a single concentric ring corresponding to the (002) reflection, consistent with the polycrystalline nature of the sample.

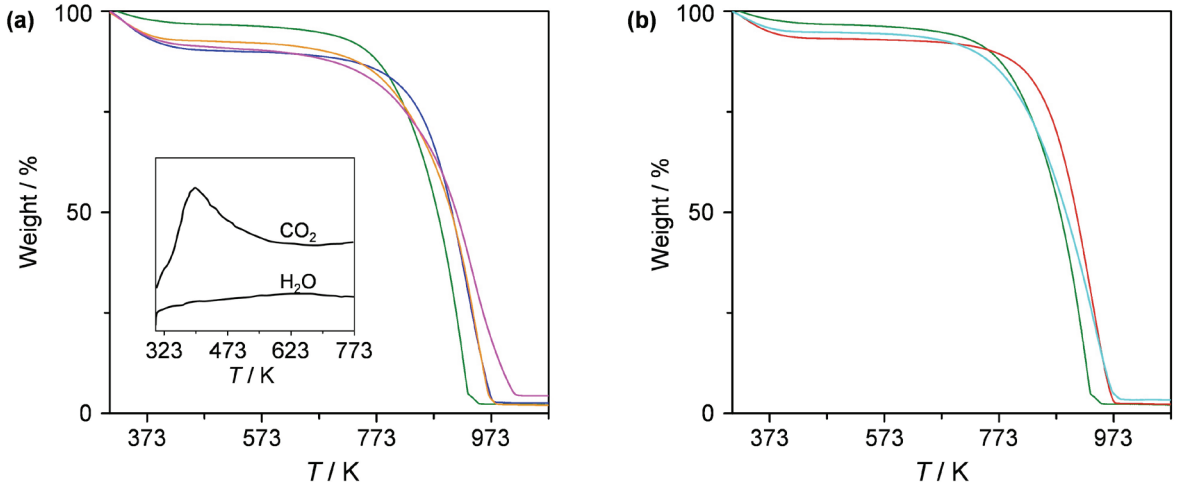

Figure S6. Thermogravimetric analysis profiles in nitrogen for the mesoporous C-doped carriers modified with BA (a) and TAP (b) and representative mass spectrometry curves (inset). The colour code as in the Fig. 4.

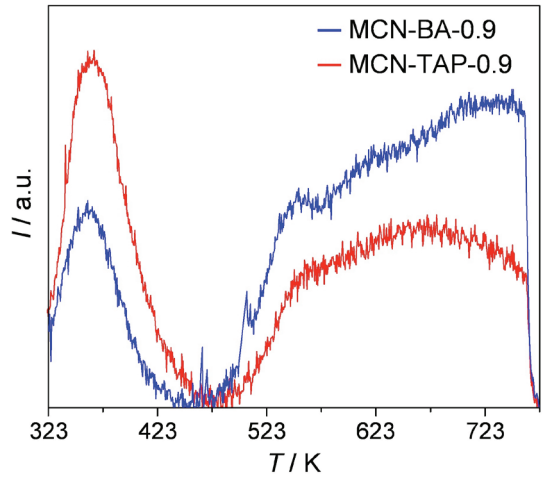

Figure S7. Temperature-programmed desorption of CO_2 ($m/z = 44$ amu) of MCN-BA-0.9 and MCN-TAP-0.9.

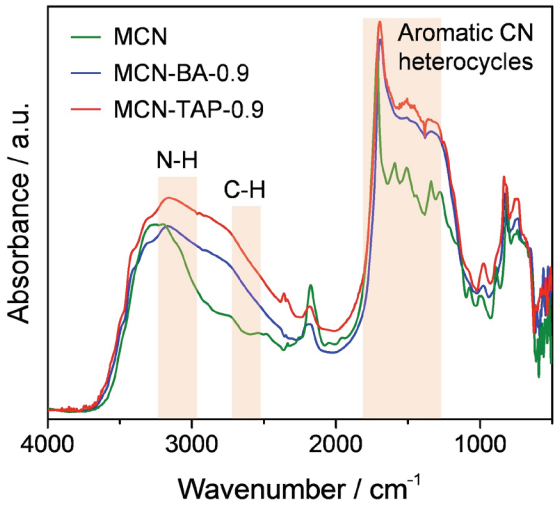

Figure S8. Diffuse reflectance infrared Fourier transform spectra of MCN, MCN-BA-0.9 and MCN-TAP-0.9 after degasification under a N_2 flow at 573 K.

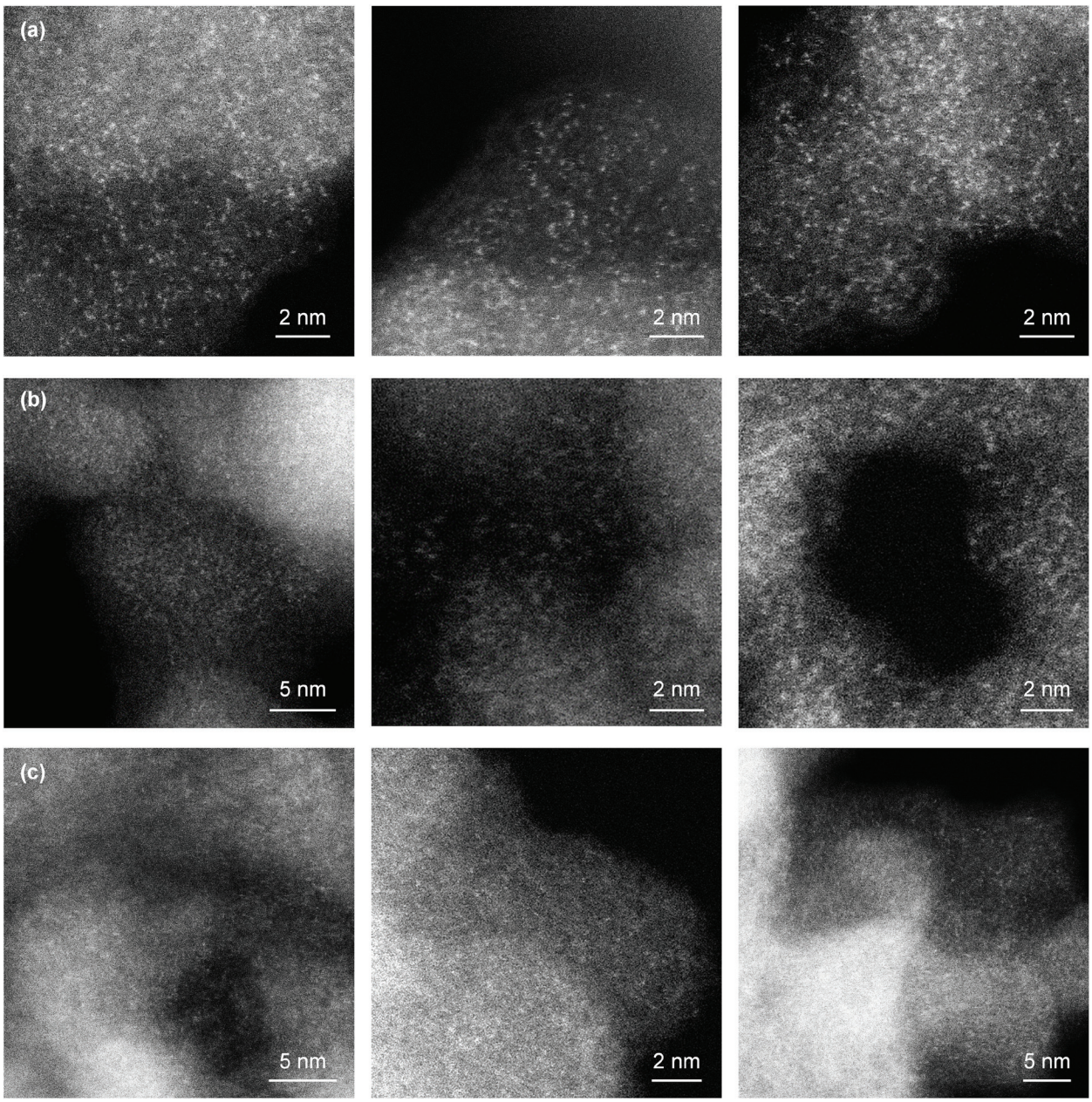

Figure S9. Aberration corrected scanning transmission electron microscopy images evidencing the Pd dispersion at further locations in (a) Pd-MCN-BA-0.9, (b) Pd-MCN-TAP-0.9 and (c) Pd-MCN. The metal is atomically dispersed and uniformly distributed over the carriers in all cases.

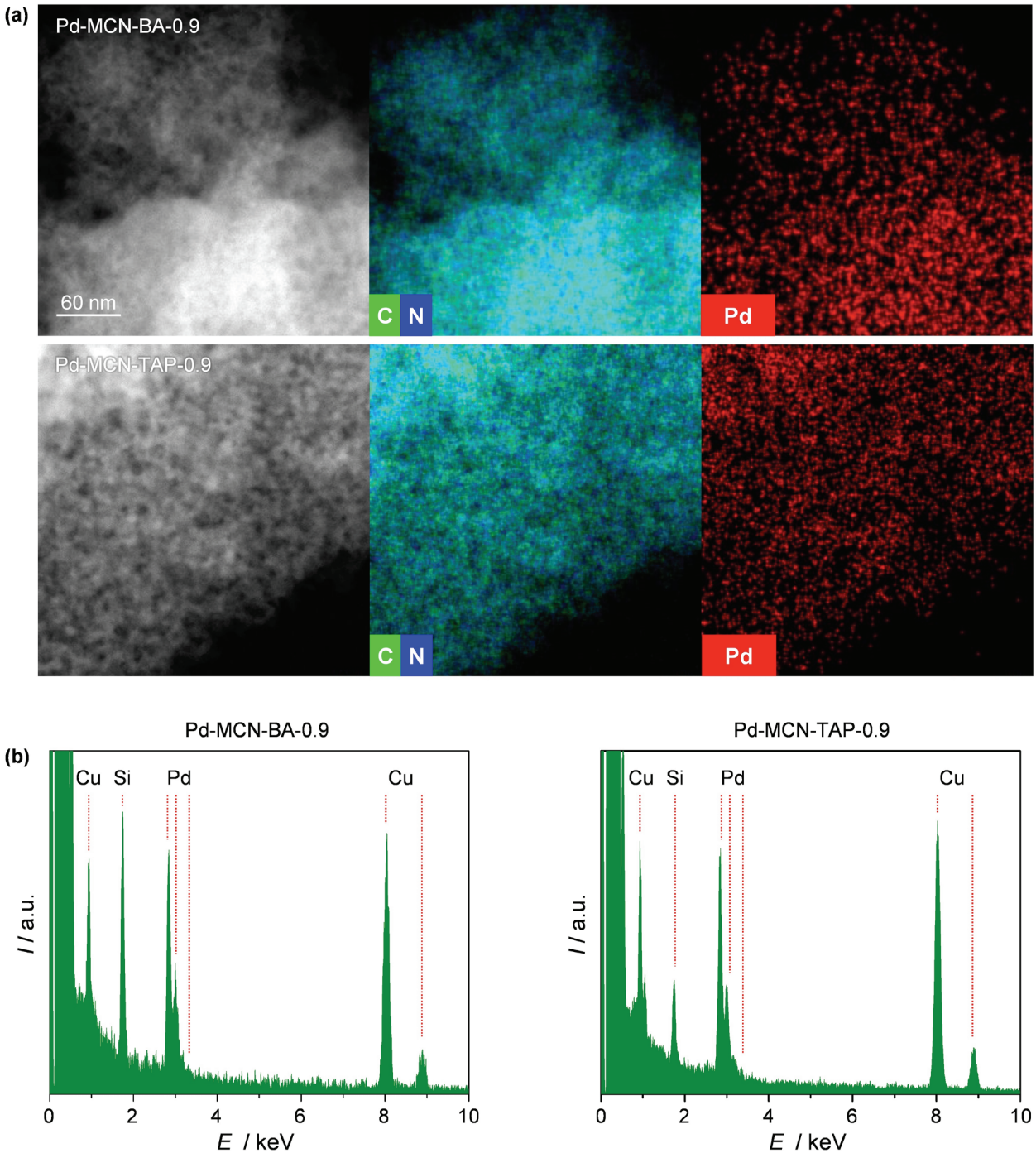

Figure S10. (a) High-angle annular dark field scanning transmission electron microscopy image and elemental maps acquired by energy dispersive X-ray spectroscopy and (b) corresponding energy-dispersive X-ray spectra of Pd-MCN-BA-0.9 and Pd-MCN-TAP-0.9. The Pd signal is clearly distinguished in both cases. The Cu signal stems from the copper grid used to support the sample. The Si signal most likely comes from the silicon drift detector used for data acquisition.

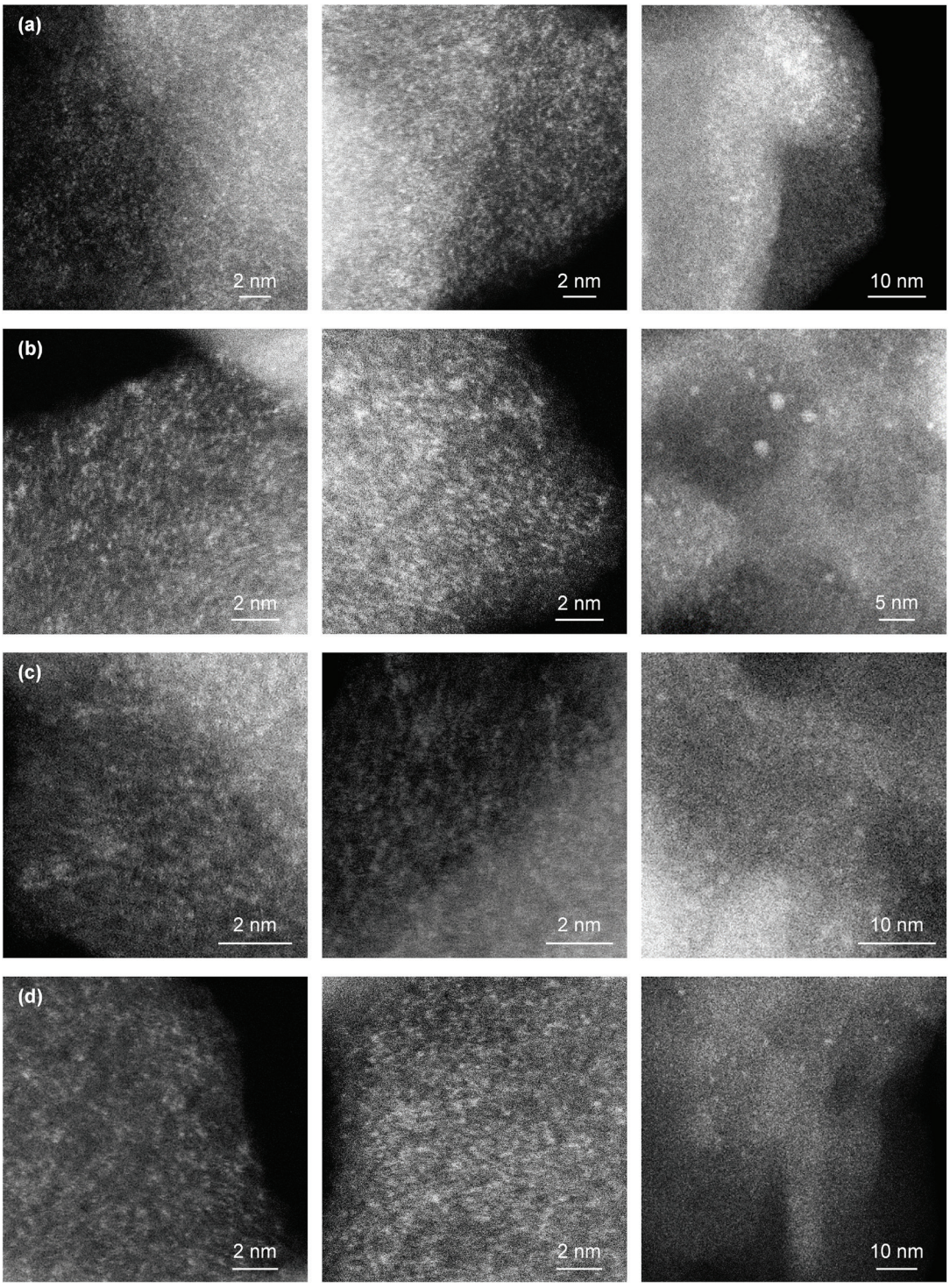

Figure S11. Aberration-corrected scanning transmission electron micrographs evidencing the Pd dispersion at further locations in (a) Pd-BCN-BA-0.9, (b) Pd-BBA, (c) Pd-BTAP and (d) Pd-BCN. Single atoms, clusters and nanoparticles can be observed in differing amounts in each case.

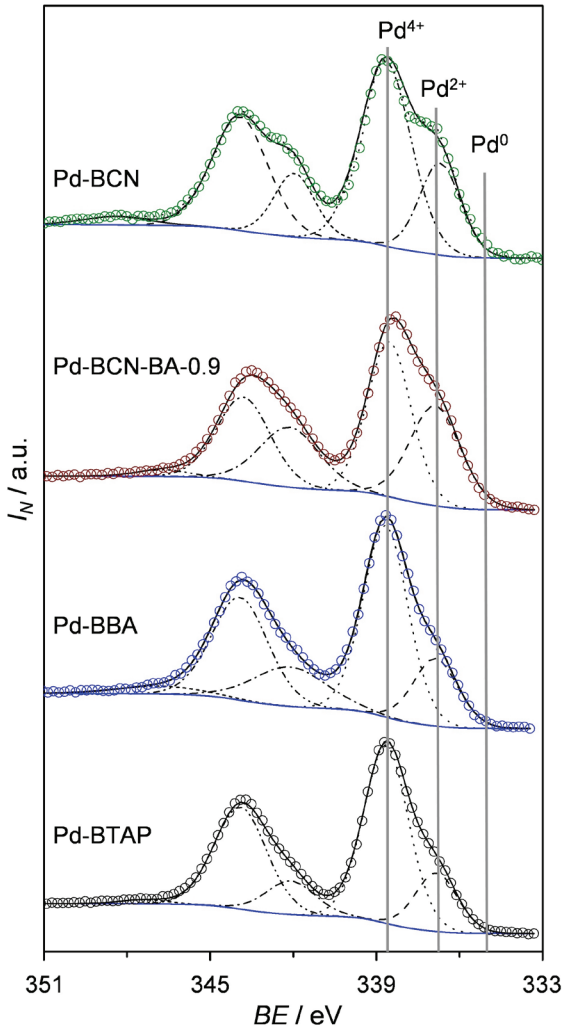

Figure S12. Comparison of the Pd 3*d* core level X-ray photoelectron spectroscopy spectra of the catalysts based on the bulk carriers. Solid black lines show the result of fitting the raw data (open symbols), the dashed lines correspond to the individual peaks after deconvolution. Blue lines indicate the background applied. Vertical grey lines indicate the positions of the deconvoluted components.

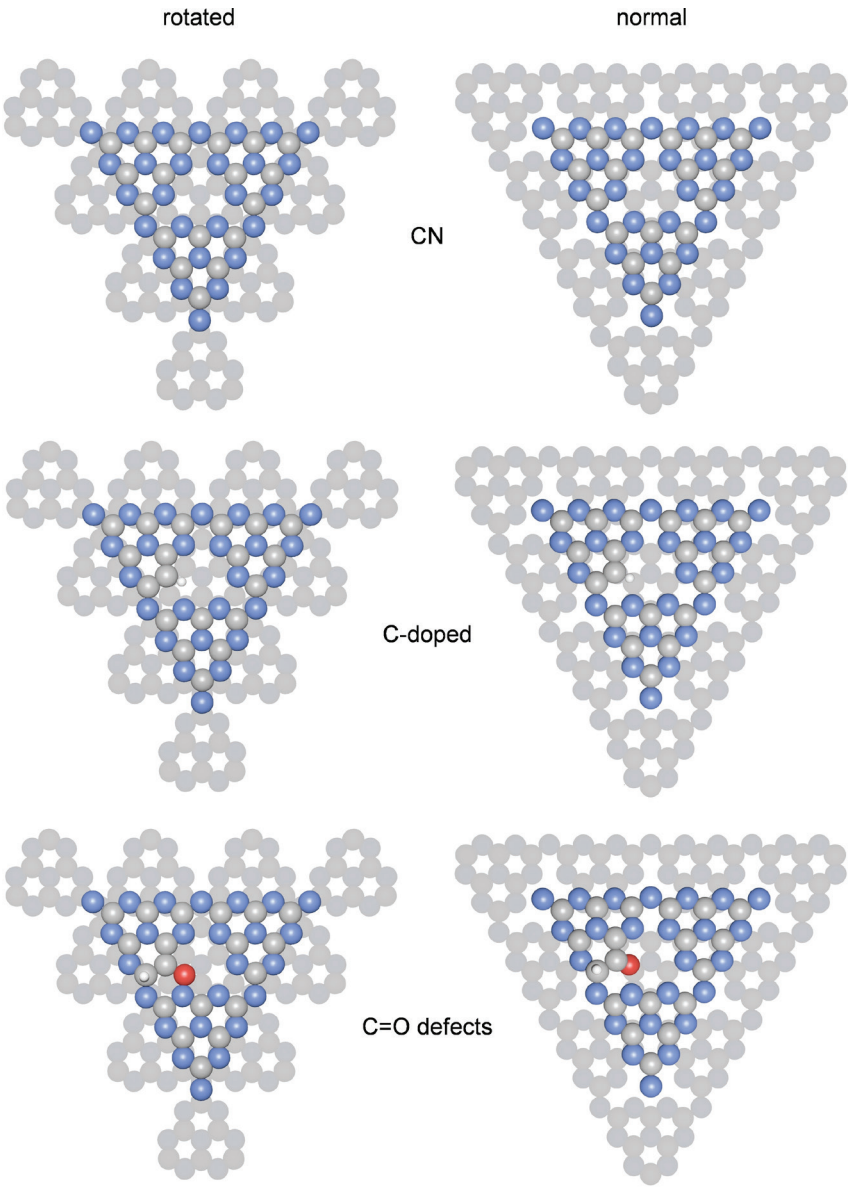

Figure S13. Lattice models of the stoichiometric and carbon-doped g-C_3N_4 carriers. Two possible stacking arrangements were considered for the binding sites defined by the tri-*s*-triazine units, normal and rotated. In these models, chemical defects have been introduced into the surface layer, replacing N atoms for CH to represent the ideal incorporation of carbon, and CO and a nearby H to represent a possible oxygen-containing defect. Colour code: grey - C, blue - N, red - O and white - H.

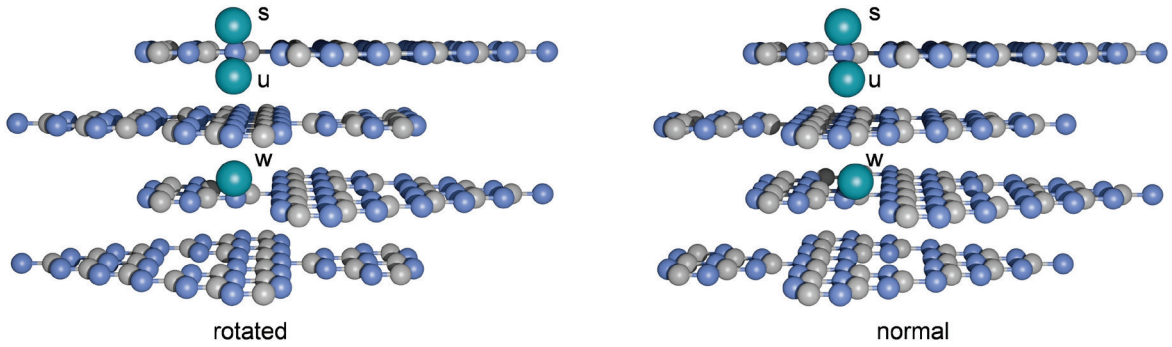

Figure S14. Metal adsorption has been considered on the surface, s, at subsurface u or at the sub-subsurface, w, in the normal and rotated g-C_3N_4 structures considered. Colour code: grey - C, blue - N and green - Pd.

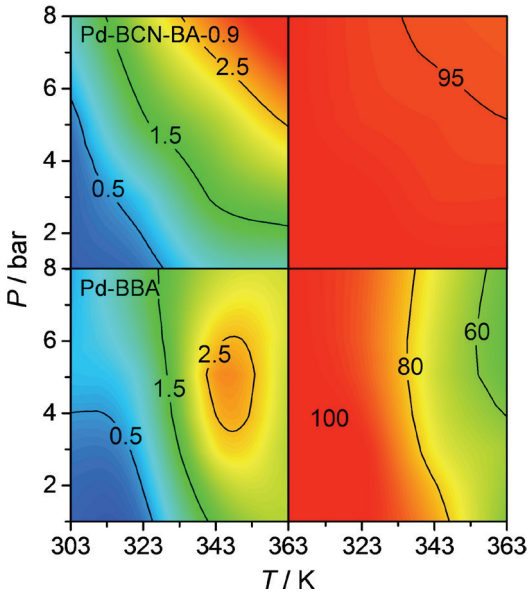

Figure S15. Reaction rate (left column, in 10^3 $mol_{2\text{-methyl-3-buten-2-ol}}$ mol_{Pd}^{-1} h^{-1}) and selectivity to 2-methyl-3-buten-2-ol (right column, in %) at different temperature and pressure over Pd-BCN-BA-0.9 and Pd-BBA. The contour plots were obtained through spline interpolation of 14 experimental points. Reaction conditions: W_{cat} = 0.1 g, F_L (2-methyl-3-butyn-2-ol + toluene) = 1 cm^3 min^{-1} and F_G (H_2) = 36 cm^3 min^{-1}.